



HAL
open science

A twofold approach in loss reduction of $\text{KTa}_{0.5}\text{Nb}_{0.5}\text{O}_3$ ferroelectric layers for low loss tunable devices at microwaves

Fatou Cissé, Xavier Castel, Ronan Sauleau, Ratiba Benzerga, Stéphanie Députier, Valérie Bouquet, Maryline Guilloux-Viry

► **To cite this version:**

Fatou Cissé, Xavier Castel, Ronan Sauleau, Ratiba Benzerga, Stéphanie Députier, et al.. A twofold approach in loss reduction of $\text{KTa}_{0.5}\text{Nb}_{0.5}\text{O}_3$ ferroelectric layers for low loss tunable devices at microwaves. *IEEE Transactions on Ultrasonics, Ferroelectrics and Frequency Control*, 2018, 65 (4), pp.665-671. 10.1109/TUFFC.2018.2795108 . hal-01685672

HAL Id: hal-01685672

<https://hal.science/hal-01685672>

Submitted on 4 Oct 2018

HAL is a multi-disciplinary open access archive for the deposit and dissemination of scientific research documents, whether they are published or not. The documents may come from teaching and research institutions in France or abroad, or from public or private research centers.

L'archive ouverte pluridisciplinaire **HAL**, est destinée au dépôt et à la diffusion de documents scientifiques de niveau recherche, publiés ou non, émanant des établissements d'enseignement et de recherche français ou étrangers, des laboratoires publics ou privés.

A Twofold Approach in Loss Reduction of $\text{KTa}_{0.5}\text{Nb}_{0.5}\text{O}_3$ Ferroelectric Layers for Low Loss Tunable Devices at Microwaves

Fatou Cissé, Xavier Castel, Ronan Sauleau, *Senior Member, IEEE*, Ratiba Benzerga, Stéphanie Députier, Valérie Bouquet and Maryline Guilloux-Viry

Abstract—Ferroelectric oxide films are attractive to design and fabricate reconfigurable and miniaturized planar devices operating at microwaves due to the large electric field dependence of their dielectric permittivity. In particular, $\text{KTa}_{1-x}\text{Nb}_x\text{O}_3$ (KTN) ferroelectric material presents a high tunability under moderate DC bias electric field. However, its intrinsic dielectric loss strongly contributes to the global loss of the related devices and limits their application areas at microwaves. In this work, a twofold approach is investigated to reduce the device loss. The intrinsic loss of KTN is firstly reduced by doping the ferroelectric material with a low loss dielectric material, namely MgO. Second, the doped ferroelectric films are confined using an original laser micro-etching process. Both routes have been implemented here to provide a synergic effect on the total insertion loss of the microwave test device, namely a coplanar waveguide stub resonator. The experimental data demonstrate a decrease of the intrinsic loss by a factor ~ 2 and a decrease of the global loss by a factor ~ 4 with a frequency tunability close to 10% at ~ 10 GHz under a moderate biasing (80 kV/cm).

Index Terms—Ferroelectric oxide, global loss, laser etching, MgO doping, tunability.

I. INTRODUCTION

THE development of tunable devices has increased significantly over the last decade, thereby facilitating implementation and access to emerging communication standards. Current reconfigurable devices mainly rely on PIN diodes [1], [2], microelectromechanical system (RF-MEMS) switches [3], [4], or field effect transistor (FET) switches [5]. But current progress in ferroelectric thin films has demonstrated their relevance for tunable devices at microwaves [6], [7]. Indeed, ferroelectric materials exhibit large dielectric permittivity ϵ_r values which can be significantly tuned under driving static electric fields. Moreover, ferroelectric thin films allow a significant

miniaturization of the microwave devices [7].

Besides the most popular ferroelectric materials, namely the well-known barium strontium titanate family $\text{Ba}_x\text{Sr}_{1-x}\text{TiO}_3$ (BST) [8] and the lead zirconate titanate family $\text{PbZr}_x\text{Ti}_{1-x}\text{O}_3$ (PZT) [9], the alternative potassium tantalate niobate family $\text{KTa}_{1-x}\text{Nb}_x\text{O}_3$ (KTN) presents relevant features at microwaves, e.g. [10], [11]. Its Curie temperature T_c can be adjusted by controlling the Nb/Ta atomic ratio. The present work focuses specifically on the $\text{KTa}_{0.5}\text{Nb}_{0.5}\text{O}_3$ composition ($x = 0.5$) which exhibits the highest agility of the dielectric permittivity [12], and thereby the largest frequency agility [13]. Its Curie temperature T_c equals 97°C (bulk value) [10]. Therefore $\text{KTa}_{0.5}\text{Nb}_{0.5}\text{O}_3$ films are expected to be in the ferroelectric state at room temperature. At microwave frequencies, it is worth noting that the loss due to the ferroelectric domain walls dynamics as well as hysteretic properties tends to disappear, offering no undue advantage to ferroelectric materials in their paraelectric state [14]. Although $\text{KTa}_{0.5}\text{Nb}_{0.5}\text{O}_3$ films exhibit high values of dielectric permittivity ($\epsilon_r \approx 700\text{--}850$ [13]), their applications at microwaves are still limited due to their significant intrinsic dielectric loss ($\tan\delta_r \approx 0.3$ at 10 GHz) [13]. Various solutions have already been investigated to lower the intrinsic loss of the material itself or the insertion loss of the related device: (i) use of a seed layer to improve the KTN crystalline quality [15], (ii) doping of KTN with iron [16], titanium [17] or MgO [18], (iii) deposition of ferroelectric/dielectric multilayers [19], (iv) ferroelectric material localization to reduce the insertion loss of the tunable devices printed on such films [20], [21], [22]. In this paper, a twofold and complementary approach is investigated to further reduce the total loss (intrinsic loss and insertion loss). The first route focuses on the MgO doping of KTN film, whereas the second one consists in confining the doped-ferroelectric layer only in regions of interest on the device layout and to remove it in non-critical areas by an original laser micro-etching process. Consequently, intrinsic loss and insertion loss can be reduced at the same time. For this purpose, simple test devices, namely three coplanar waveguide (CPW) transmission lines and a CPW stub resonator, have been designed and characterized in X-band to demonstrate the relevance of the twofold approach.

The paper is organized as follows. The device fabrication process is described in Section II, and the impact of MgO

F. Cissé, X. Castel, R. Sauleau, and R. Benzerga are with the Institut d'Electronique et de Télécommunications de Rennes, UMR CNRS 6164, Université de Rennes 1, 35042 Rennes, France (e-mail: xavier.castel@univ-rennes1.fr).

S. Députier, V. Bouquet, and M. Guilloux-Viry are with the Institut des Sciences Chimiques de Rennes, UMR CNRS 6226, Université de Rennes 1, 35042 Rennes, France (e-mail: maryline.guilloux-viry@univ-rennes1.fr).

doping and confinement of KTN films are investigated experimentally in Section III. Finally, conclusions are drawn in Section IV.

II. FABRICATION PROCESS OF THE DEVICES

A. Elaboration of the undoped and doped KTN films

The KTN thin films were grown by pulsed laser deposition (KrF excimer laser; $\lambda = 248$ nm) at 700°C under an oxygen pressure of 30 Pa on R-plane sapphire substrates ($10\text{ mm} \times 10\text{ mm} \times 0.5\text{ mm}$). The KrF excimer laser was operated at 2 Hz with a fluence of 2 J/cm^2 . Three home-made $\text{KTa}_{0.5}\text{Nb}_{0.5}\text{O}_3$ targets (undoped, doped with 3% MgO in mol. and doped with 6% MgO in mol.) were used for the deposition of the KTN films. An excess of potassium (60% KNO_3 in mol.) in the targets was used to overcome the volatility of the alkali element during the deposition stage. The undoped KTN, 3% MgO doped KTN, and 6% MgO doped KTN films have a thickness equal to 600 nm, 530 nm, and 700 nm respectively. A polycrystalline growth preferentially oriented (100) was observed by X-ray diffraction (XRD) analysis (Fig. 1). The 3% MgO doped KTN film exhibits a very small amount of KTN pyrochlore phase. This secondary phase is favored by a slight potassium deficiency, which is generally avoided by the use of KNO_3 enriched targets. The surface morphologies (Fig. 2) observed by scanning electron microscopy (SEM) of the undoped and doped films are consistent with the polycrystalline growth shown by XRD. The presence of areas with uniformly oriented grains demonstrates the preferentially oriented growth of such layers. The grains with parallelepiped shape are characteristic of the (100) orientation (Fig. 2a). Grains with rounded edges are observed on the doped films (Figs. 2b and 2c). This phenomenon is still unclear.

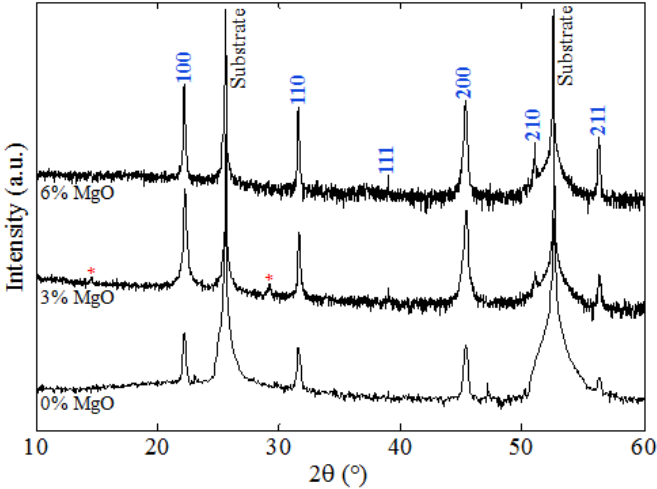


Fig. 1. θ - 2θ XRD patterns of the undoped KTN film, 3%-MgO doped KTN film, and 6%-MgO doped KTN film. The red asterisk (*) is related to the pyrochlore phase.

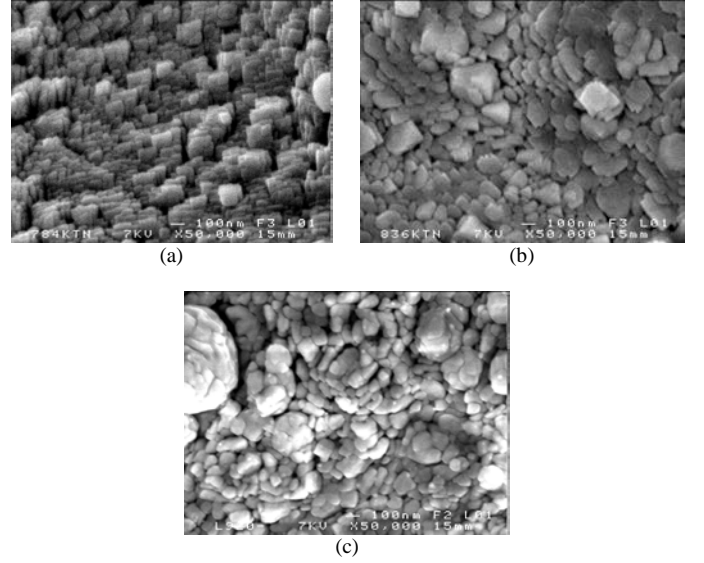


Fig. 2. Scanning Electron Microscopy plane views of (a) undoped KTN film, (b) 3%-MgO doped KTN film, and (c) 6%-MgO doped KTN film.

B. Design and fabrication of the test devices

Two types of devices have been specifically designed for this study by using a 3-D commercial electromagnetic software (Ansys HFSSTM). They are fabricated on 0.5 mm thick sapphire substrates ($\epsilon_r = 10$; $\tan\delta = 10^{-4}$). Three 50- Ω CPW transmission lines of different lengths (3 mm, 5 mm and 8 mm) have been selected to assess precisely the dielectric characteristics of the undoped and doped KTN films. Each line is $40\text{ }\mu\text{m}$ wide (w_l) and is surrounded by a gap g_l of $50\text{ }\mu\text{m}$ (Fig. 3). The second type of devices is a CPW quarter-wavelength open-ended stub resonator (Fig. 3). Its resonance frequency F_r depends on the effective permittivity of the heterostructure, as follows:

$$F_r = \frac{c}{4L_r \sqrt{\epsilon_{eff}}} \quad (1)$$

where L_r , c , and ϵ_{eff} are the stub length, the speed of light in vacuum, and the effective permittivity of the heterostructure, respectively. This resonator has been designed to operate in X-band (~ 10 GHz).

The RF magnetron sputtering technique was used to fabricate the samples. A bilayer of 5 nm-thick titanium and 2 μm -thick silver was deposited on each KTN layer at room temperature. The titanium underlayer was used here only to ensure the strong adhesion of the silver overlayer onto the ferroelectric oxide. The silver thickness was set at three times the skin depth value at 10 GHz ($\delta = 0.64\text{ }\mu\text{m}$). Subsequently a standard photolithographic wet etching process with the appropriate photomask was used to pattern the devices. The nominal dimensions of the three transmission lines and of the stub resonator are provided in Fig. 3. Finally, gold wire bondings (length: $\sim 250\text{ }\mu\text{m}$, diameter: $25\text{ }\mu\text{m}$, black rectangles in Fig. 3) were used to enforce the equipotential condition on both CPW grounds and to prevent from the excitation of parasitic slotline modes.

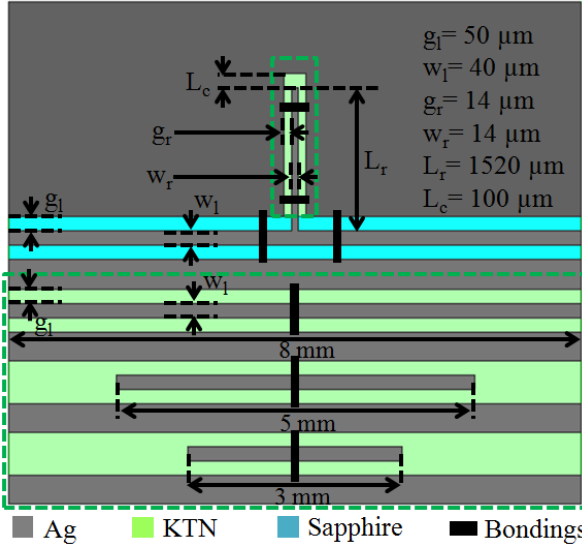


Fig. 3. Layout and dimensions of the CPW devices. The grey areas correspond to the metallic pattern. The green dashed lines define the area with KTN after laser micro-etching.

C. Confinement by laser micro-etching

The devices fabricated in Section II.B were printed on KTN films covering the entire substrate area (Fig. 4a). Once experimentally characterized in reflection and transmission, the same samples have been used in a second step to study the impact of KTN confinement on the device performance. To this end, the titanium and silver bilayers were first fully removed by chemical wet etching. Then, the laser micro-etching technique [20], [23], [24] was implemented to confine the ferroelectric layer only underneath and close to the CPW resonator; KTN was removed in non-critical areas (i.e. underneath the ground plane and the feeding line of the stub, see Fig. 3). The same wavelength was used for KTN deposition and KTN micro-etching (KrF , $\lambda = 248 \text{ nm}$). Indeed, KTN material interacts efficiently with KrF laser beam due to its optical band gap ($E_g = 4.1 \text{ eV}$) lower than the photon energy and its high absorption coefficient ($\alpha > 200\,000 \text{ cm}^{-1}$ at 248 nm), even after doping. Moreover, sapphire substrate is almost transparent at this working wavelength. The optimal parameters of the laser etching were determined to obtain a clean surface without damaging the substrate. A laser fluence of $\sim 1.2 \text{ J/cm}^2$, a frequency of 60 Hz , a $500 \mu\text{m} \times 500 \mu\text{m}$ laser spot size with ~ 400 laser shots/area coupled to controlled micrometric displacements of the sample under the laser beam (workstation with X-Y tables) were used to properly confine the ferroelectric films. An exact sizing of the non-etched KTN area ($100 \mu\text{m} \times 1620 \mu\text{m}$) was then obtained. The width of the KTN tape ($100 \mu\text{m}$) is large enough to confine most of the field lines in the stub region. To finalize the fabrication of the devices, the metallization process, photolithography and wet etching steps were implemented once more. Note that a special attention must be taken to precisely align the stub on the non-etched KTN area (Fig. 4b). To assess the impact of the different fabrication steps on the intrinsic properties of the ferroelectric materials, transmission lines were reprinted on the non-etched area of the samples (green dashed lines in

Fig. 3). The device dimensions are the same as prior to the laser micro-etching step. The measured central conductor widths and gaps of the transmission lines and stub are ($w_l = 35 \mu\text{m}$, $g_l = 55 \mu\text{m}$) and ($w_r = 14 \mu\text{m}$, $g_r = 18 \mu\text{m}$), respectively. Note that the measured dimensions of the devices are slightly different from those of the photomask (Fig. 3) due to the overetching effect attached to the wet etching process used.

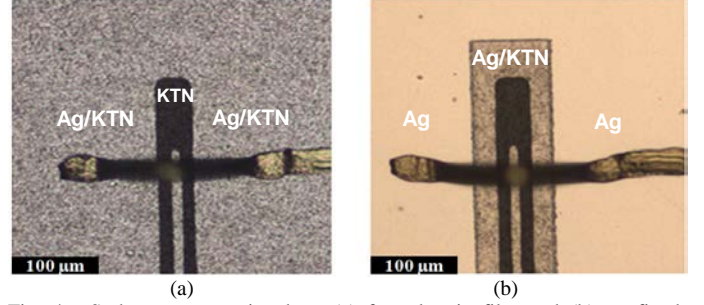


Fig. 4. Stub resonator printed on (a) ferroelectric film and (b) confined ferroelectric film after laser micro-etching (optical microscopy pictures).

III. EXPERIMENTAL RESULTS

Microwave measurements were performed from 1 GHz to 20 GHz using a vector network analyzer, two bias tees, and a probe station. A maximum DC bias voltage equal to 150 V was applied to the devices, which corresponds to a maximum static electric field of 80 kV/cm for the stub resonator and 27 kV/cm for the transmission lines. The dielectric characteristics (ϵ_r , $\tan\delta_r$) of the undoped and doped KTN films were retrieved through post-processed S_{11} and S_{21} measurements of the CPW $50\text{-}\Omega$ transmission lines using a home-made analytical model based on the conformal mapping method [13], [25].

A. Influence of MgO doping

The dielectric characteristics of the undoped and doped KTN films are represented in Fig. 5a and Fig. 6a. At 10 GHz and $E_{\text{bias}} = 0 \text{ kV/cm}$, the KTN sample doped with 3% MgO in mol. shows a decrease of ϵ_r from 860 to 355 and of $\tan\delta_r$ from 0.31 to 0.20. Under $E_{\text{bias}} = 27 \text{ kV/cm}$, ϵ_r decreases from 580 to 310 and $\tan\delta_r$ from 0.23 to 0.19. With a 6% MgO doping, the dielectric permittivity shows a similar decrease from 860 to 390, while an important loss reduction is measured: $\tan\delta_r$ is divided by a factor 2.2 ($\tan\delta_r = 0.14$ at 10 GHz and $E_{\text{bias}} = 0 \text{ kV/cm}$). The impact of the MgO doping rate is therefore not significant for ϵ_r , in contrast to $\tan\delta_r$. The given values are summarized in Table I. Similar results (per unit length) have been obtained with the three $50\text{-}\Omega$ CPW lines (not given here); this underlines the good homogeneity in thickness and composition of the undoped and doped KTN films. The 6% MgO doping is therefore the better trade-off to reduce significantly the intrinsic loss of KTN thin films while keeping up a high permittivity value. The slow decrease of ϵ_r versus frequency is in accordance with the restriction of the dynamic polarization mechanisms of KTN due to the doping effect. The fast decrease of $\tan\delta_r$ from 1 GHz to 5 GHz has

been attributed to the freezing of polar domain motion and to the restriction to the metal skin depth loss [13]. Note also that MgO doping reduces frequency dispersion (Figs. 6a and 6b).

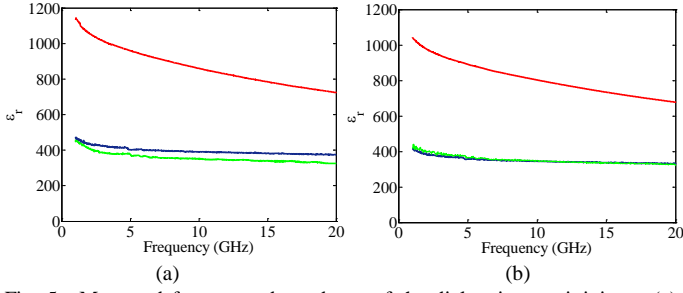


Fig. 5. Measured frequency dependence of the dielectric permittivity ϵ_r (a) before and (b) after KTN confinement. Red line: undoped KTN; green line: 3%-MgO doped KTN; blue line: 6%-MgO doped KTN at $E_{bias} = 0$ kV/cm.

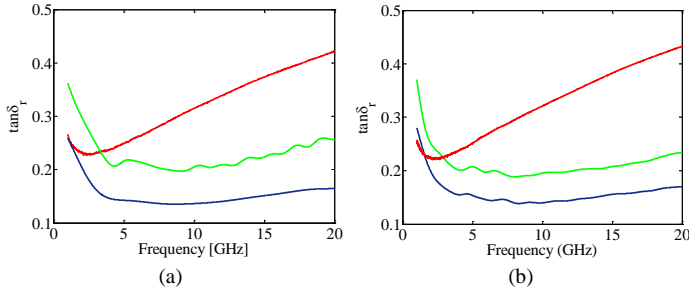


Fig. 6. Measured frequency dependence of the loss tangent $\tan \delta_r$ (a) before and (b) after KTN confinement. Red line: undoped KTN; green line: 3%-MgO doped KTN; blue line: 6%-MgO doped KTN at $E_{bias} = 0$ kV/cm.

The resulting variation of ϵ_r and $\tan \delta_r$ by doping could be explained by: (i) an improvement of the film microstructure (not observed here by XRD measurement); (ii) the addition in KTN material of a low permittivity and low loss dielectric phase material, namely MgO; (iii) a shift of the T_c value down to lower temperature inducing the paraelectric state of the doped KTN films at room temperature. A previous study based on the doped $\text{BaZr}_{0.25}\text{Ti}_{0.75}\text{O}_3$ material had demonstrated a decrease of the Curie temperature due to the addition of MgO [26]. Another study had shown a decrease of the T_c value by MgO doping of the KTN thin films. A shift of about 30 K was observed with a 3% MgO doped KTN film in a Metal-Insulator-Metal (MIM) heterostructure characterized at lower frequencies (100 kHz - 1 MHz) [27]. Indeed, in the present work, the variation of the measured stub resonance frequency F_r versus biasing shows a hysteretic behavior for the undoped KTN sample (Fig. 7a), highlighted by a higher F_r value reached at the end of the cycle hysteresis (0 kV/cm \rightarrow 80 kV/cm \rightarrow 0 kV/cm \rightarrow -80 kV/cm \rightarrow 0 kV/cm), whereas no hysteretic behavior with an identical final F_r value is observed for the 6% MgO doped KTN film (Fig. 7b). In our opinion, that is typical of a ferroelectric/paraelectric state transition caused by MgO doping.

TABLE I
DIELECTRIC PERMITTIVITY ϵ_r , LOSS TANGENT $\tan \delta_r$, GLOBAL LOSS GL , AND TUNABILITY T OF THE UNDOPED AND DOPED KTN FILMS

	$E_{bias} = 0$ kV/cm				$E_{bias} = 27$ kV/cm		$E_{bias} = 80$ kV/cm		
	@		@		@		@		
	10 GHz		F_r		10 GHz		F_r		
	ϵ_r	$\tan \delta_r$	F_r	GL	ϵ_r	$\tan \delta_r$	F_r	GL	T (%)
KTN	860	0.31	9.4	0.73	580	0.23	13.5	0.72	44
3% MgO doped KTN	355	0.20	12.2	0.61	310	0.19	13.8	0.56	11
6% MgO doped KTN	390	0.14	12.3	0.54	370	0.14	13.6	0.52	11

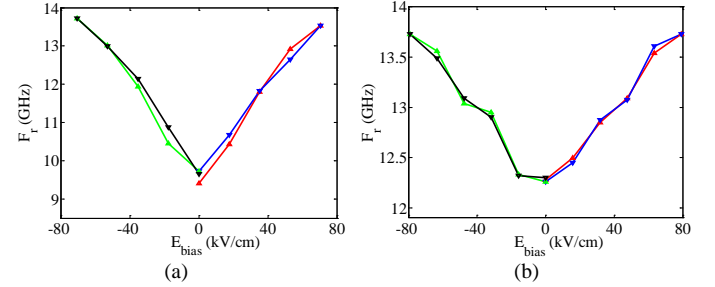


Fig. 7. Variation of the stub resonance frequency F_r versus biasing of the (a) undoped KTN film and (b) 6%-MgO doped KTN film.

The decrease of the permittivity values due to MgO doping reduces the frequency tunability T of the printed stub resonator (Table I). Here T is defined as the relative variation of the resonance frequency under the applied DC bias electric field E_{bias} , as follows [28]:

$$T(\%) = \frac{|F_r(E_{bias} = 0) - F_r(E_{bias})|}{F_r(E_{bias} = 0)} \times 100 \quad (2)$$

where $F_r(E_{bias})$ and $F_r(E_{bias}=0)$ are the resonance frequencies with and without E_{bias} , respectively (Fig. 8). Under biasing, the resonance frequency of the undoped film shifts from 9.4 to 13.5 GHz. By doping the KTN with 3% and 6% MgO in mol., we observe respectively a shift from 12.2 to 13.8 GHz and a shift from 12.3 to 13.6 GHz. The decrease of the dielectric permittivity by doping leads to an increase of the resonance frequency. The tunability decreases from 44% to 11% (Table I and Fig. 9a), with a significant global loss reduction (GL) from 0.72 to 0.56 (3%-MgO) and 0.52 (6%-MgO) (Table I and Fig. 10a). The global loss is defined as follows:

$$GL = 1 - |S_{11}|^2 - |S_{21}|^2 \quad (3)$$

These results strongly confirm the previous ones coming from the variation of the intrinsic dielectric characteristics of the KTN films accordingly to MgO doping.

MgO doping causes a concomitant reduction of the permittivity and tunability in most cases. In a MIM capacitor configuration at 100 kHz, the reduction of permittivity (from 720 to 334) and tunability (from 28% to 17.2% under $E_{bias} = 237$ kV/cm) by doping $\text{Ba}_{0.6}\text{Sr}_{0.4}\text{TiO}_3$ thin films with 5%

Mg in mol. was described in [29]. $\tan\delta_r$ value decreased too, from 0.1 to 0.007. Another study reported the variation of (ϵ_r , $\tan\delta_r$, tunability under $E_{bias}=444$ kV/cm) values from (360, 0.013, 65.5%) to (320, 0.009, 29%) by doping multilayered $Ba_xSr_{1-x}TiO_3$ thin films with 5% MgO in mol. [30].

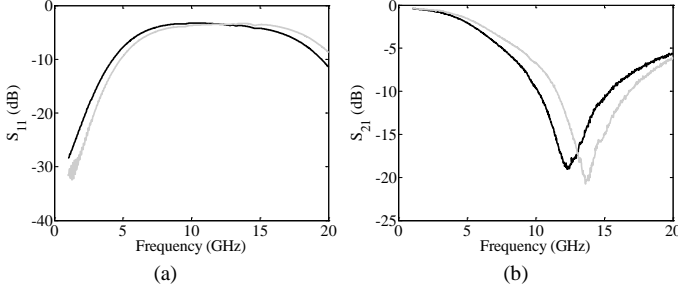


Fig. 8. Measured (a) reflection coefficient S_{11} and (b) transmission coefficient S_{21} of the stub resonator printed on the 6%-MgO doped KTN film before confinement. Black line: $E_{bias}=0$ kV/cm; grey lines: $E_{bias}=80$ kV/cm.

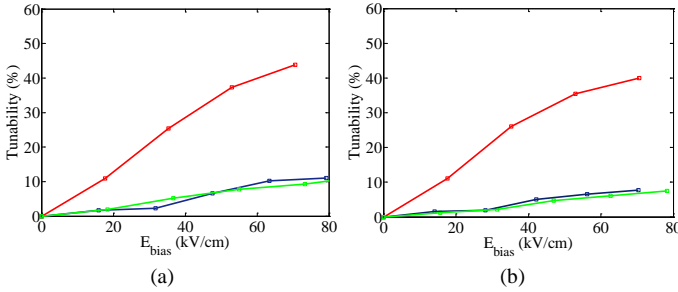


Fig. 9. Variation of the frequency tunability under biasing (a) before and (b) after KTN confinement. Red line: undoped KTN; green line: 3%-MgO doped KTN; blue line: 6%-MgO doped KTN.

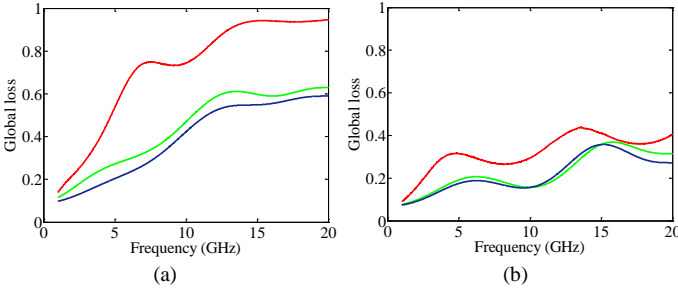


Fig. 10. Global loss versus frequency (a) before and (b) after KTN confinement. Red line: undoped KTN; green line: 3%-MgO doped KTN; blue line: 6%-MgO doped KTN at $E_{bias}=0$ kV/cm.

B. Influence of KTN confinement

To further reduce the global loss of the stub resonator devices, KTN was confined underneath the stub using laser micro-etching. The dielectric characteristics of the undoped and doped KTN films were retrieved from the transmission lines reprinted on the non-etched film area (see Fig. 3). Figs. 5 and 6 depict the variation versus frequency of the dielectric characteristics ϵ_r and $\tan\delta_r$, respectively. For example, at 10 GHz and $E_{bias}=0$ kV/cm, the weak variation of ϵ_r (from 390 to 350) and the constant value of $\tan\delta_r$, before and after the confinement of the 6% MgO doped KTN film demonstrates thereby the preservation of the dielectric properties of the oxide film after the different stages of the fabrication process,

namely the silver and titanium fully wet etching stage, the titanium and silver redeposition by RF sputtering, and the standard photolithographic wet etching process. The detailed results are summarized in Table II.

Regarding the stub resonator measurements, on one hand a slight decrease of the tunability is observed after the KTN confinement and whatever the nature of the films (undoped and doped KTN). T changes from 11% to 8% for the doped films (Fig. 9b). On the other hand, a strong reduction in the global loss is obtained (Fig. 10b). At the resonance frequency F_r and $E_{bias}=0$ kV/cm, GL of the undoped KTN decreases from 0.73 to 0.29; 0.61 to 0.26 for the 3% MgO doped KTN film and 0.54 to 0.20 for the 6% MgO doped KTN film. A global loss reduction by a factor ~ 4 is therefore achieved from the undoped KTN sample to the confined 6% MgO doped KTN film. The results are also summarized in Table II.

TABLE II
DIELECTRIC PERMITTIVITY ϵ_r , LOSS TANGENT $\tan\delta_r$, GLOBAL LOSS GL , AND TUNABILITY T AFTER LASER MICRO-ETCHING

	$E_{bias}=0$ kV/cm		$E_{bias}=27$ kV/cm		$E_{bias}=80$ kV/cm				
	@		@		@				
	10 GHz		F_r		10 GHz				
	ϵ_r	$\tan\delta_r$	F_r	GL	ϵ_r	$\tan\delta_r$	F_r	GL	T (%)
Confined KTN	805	0.32	9.4	0.29	530	0.24	13.1	0.31	40
Confined 3% MgO doped KTN	350	0.19	13.3	0.26	320	0.20	14.3	0.27	8
Confined 6% MgO doped KTN	350	0.14	12.2	0.20	330	0.14	13.2	0.25	8

IV. CONCLUSION

This study demonstrates the relevance of the proposed twofold and complementary approach to achieve low loss tunable devices at microwaves. The reduction of the intrinsic dielectric loss by MgO doping associated with the confinement of the ferroelectric material in the active area of the stub enable a significant reduction of the global loss of the microwave device. However, MgO doping induces a reduction of the dielectric permittivity value, restricting the tunability of such devices. Accordingly to the intended application, a high tunability or a strong reduction of the global loss will be achieved. This twofold approach paves the way for the design of ferroelectric reconfigurable devices with attractive performance beyond X-band.

ACKNOWLEDGMENT

The authors warmly thank S. Ollivier for her strong assistance in KTN thin films preparation. The authors are grateful for the assistance in SEM observations of the staff of the CMEBA facility (ScanMAT, UMS 2001 CNRS - Université de Rennes 1) which received a financial support from the Région Bretagne and European Union (CPER-FEDER 2007-2014, Présage n°39126 and Présage n°37339).

This work is also supported by the European Union through the European Regional Development Fund (ERDF), the Ministry of Higher Education and Research, the Région Bretagne, the Département des Côtes d'Armor and Saint-Brieuc Armor Agglomération, through the CPER Projects 2015-2020 MATECOM and SOPHIE / STIC & Ondes.

REFERENCES

- [1] Y. Pan, K. Liu, and Z. Hou, "A novel printed microstrip antenna with frequency reconfigurable characteristics for Bluetooth/WLAN/WiMAX applications," *Microw. Opt. Technol. Lett.*, vol. 55, no. 6, pp. 1341–1345, Jun. 2013.
- [2] Y. K. Bekali and M. Essaïdi, "Compact reconfigurable dual frequency microstrip patch antenna for 3G and 4G mobile communication technologies," *Microw. Opt. Technol. Lett.*, vol. 55, no. 7, pp. 1622–1626, Jul. 2013.
- [3] K. Topalli, E. Erdil, O. A. Civi, S. Demir, S. Koc, and T. Akin, "Tunable dual-frequency RF MEMS rectangular slot ring antenna," *Sens. Actuators A*, vol. 156, no. 2, pp. 373–380, Oct. 2009.
- [4] C. W. Jung, M.-J. Lee, G. P. Li, and F. De Flaviis, "Reconfigurable scan-beam single-arm spiral antenna integrated with RF-MEMS switches," *IEEE Trans. Antennas Propag.*, vol. 54, no. 2, pp. 455–463, Feb. 2006.
- [5] X.-L. Yang, J.-C. Lin, G. Chen, and F.-L. Kong, "Frequency reconfigurable antenna for wireless communications using GaAs FET switch," *IEEE Wireless Propag. Lett.*, vol. 14, pp. 807–810, Mar. 2015.
- [6] D. Cure, T. M. Weller, T. Price, F. A. Miranda, and F. W. VanKeuls, "Low-profile tunable dipole antenna using barium strontium titanate varactors," *IEEE Trans. Antennas Propag.*, vol. 62, no. 3, pp. 1185–1193, Mar. 2014.
- [7] H. V. Nguyen, R. Benzerger, C. Borderon, C. Delaveaud, A. Sharaiha, Raphael Renoud, C. Le Paven, S. Pavy, K. Nadaud, and H. Gundel, "Miniaturized and reconfigurable notch antenna based on a BST ferroelectric thin film," *Mater. Res. Bull.*, vol. 67, pp. 255–260, Jul. 2015.
- [8] H. Jiang, M. Patterson, D. Brown, C. Zhang, K. Pan, G. Subramanyam, D. Kuhl, K. Leedy, and C. Cerny, "Miniaturized and reconfigurable CPW square-ring slot antenna loaded with ferroelectric BST thin film varactors," *IEEE Trans. Electron Devices*, vol. 60, pp. 3111–3119, Jul. 2012.
- [9] K. Aljonubi, A. O. AlAmoudi, R. J. Langley, and I. Reaney, "Reconfigurable antenna using smart material," in *7th Eur. Conf. Antennas Propag. (EuCAP)*, Gothenburg, Sweden, Apr. 2013, pp. 917–918.
- [10] D. Rytz, A. Châtelain, and U. T. Höchli, "Elastic properties in quantum ferroelectric $\text{KTa}_{1-x}\text{Nb}_x\text{O}_3$," *Phys. Rev. B*, vol. 27, no. 11, pp. 6830–6840, Jun. 1983.
- [11] A. C. Carter, J. S. Horwitz, D. B. Chrisey, J. M. Pond, S. W. Kirchoefer, W. Chang, "Pulsed laser deposition of ferroelectric thin films for room temperature active microwave electronics," *Integr. Ferroelectr.*, vol. 17, no. 1-4, pp. 273–285, Aug. 1997.
- [12] A. Perrin, A. Rousseau, D. Fasquelle, V. Laur, V. Bouquet, S. Députier, P. Laurent, G. Tanné, F. Huret, J.C. Carru, and M. Guilloux-Viry, "Epitaxially grown ferroelectric thin films for agile devices," *Phase Transitions*, Vol. 81, nos 7–8, pp. 643–665, Jul./Aug. 2008.
- [13] Q. Simon, Y. Corredores, X. Castel, R. Benzerger, R. Sauleau, K. Mahdjoubi, A. Le Febvrier, S. Députier, and M. Guilloux-viry, L. Zhang, P. Laurent, and G. Tanné, "Highly tunable microwave stub resonator on ferroelectric $\text{KTa}_{0.5}\text{Nb}_{0.5}\text{O}_3$ thin film," *Appl. Phys. Lett.*, vol. 99, no. 9, p. 092904, Aug. 2011.
- [14] S. S. Gevorgian and E. L. Kollberg, "Do we really need ferroelectrics in paraelectric phase only in electrically controlled microwave devices?" *IEEE Trans. Microw. Theory Techn.*, vol. 49, no. 11, pp. 2117–2124, Nov. 2001.
- [15] J.-M. Le Floch, F. Houndonougbo, V. Madrangeas, D. Cros, M. Guilloux-Viry, and W. Peng, "Thin film materials characterization using TE modes cavity," *J. Electromagn. Waves Appl.*, vol. 23, no. 4, pp. 549–559, Feb. 2009.
- [16] Y. M. Abdulraheem, A. L. Gentile, and O. M. Stafuss, "The effects of iron as a dopant on the dielectric properties of ferroelectric potassium tantalate niobate ($\text{KTa}_x\text{Nb}_{1-x}\text{O}_3$)," *J. Appl. Phys.*, vol. 100, p. 104111, Jul. 2006.
- [17] H.-J. Bae, J. Sigman, D. P. Norton, and L. Boatner, "Dielectric properties of Ti-doped $\text{K}(\text{Ta,Nb})\text{O}_3$ thin films grown by pulsed laser deposition," *Mater. Sci. Eng.: B*, vol. 117, no. 1, pp. 87–91, Feb. 2005.
- [18] Q. Simon, V. Bouquet, W. Peng, J.-M. Le Floch, F. Houndonougbo, S. Députier, S. Weber, A. Dauscher, V. Madrangeas, D. Cros, M. Guilloux-Viry, "Reduction of microwave dielectric losses in $\text{KTa}_{1-x}\text{Nb}_x\text{O}_3$ thin films by MgO-doping," *Thin Solid Films*, vol. 517, pp. 5940–5942, Aug. 2009.
- [19] Y. Corredores, A. Le Febvrier, X. Castel, R. Sauleau, R. Benzerger, S. Députier, M. Guilloux-Viry, A. Mekadmi, N. Martin, and G. Tanné, "Study of ferroelectric/dielectric multilayers for tunable stub resonator applications at microwaves," *Thin solid films*, vol. 553, pp. 109–113, Feb. 2014.
- [20] Y. Corredores, Q. Simon, R. Benzerger, X. Castel, R. Sauleau, A. Le Febvrier, S. Députier, M. Guilloux-Viry, L. Zhang, and G. Tanné, "Loss reduction technique in ferroelectric tunable devices by laser microetching. Application to a CPW stub resonator in X-Band," *IEEE Trans. Electron Devices*, vol. 66, pp. 4166–4170, Sep. 2014.
- [21] F. A. Miranda, G. Subramanyam, F. W. Van Keuls, R. R. Romanofsky, J. D. Warner, and C. H. Mueller, "Design and development of ferroelectric tunable microwave components for Ku and K-band satellite communication systems," *IEEE Trans. Microw. Theory Techn.*, vol. 48, no. 7, pp. 1181–1189, Jul. 2000.
- [22] S. Pavy, C. Borderon, S. Baron, R. Renoud, H. W. Gundel, "Study of wet chemical etching of BaSrTiO_3 ferroelectric thin films for intelligent antenna application," *J. Sol-Gel Sci. Technol.*, vol. 74, pp. 507–512, Jan. 2015.
- [23] G. Legeay, X. Castel, R. Benzerger, and J. Pinel, "Excimer laser beam/TiO interaction: From laser processing to surface reaction," *Phys. Status Solidi C*, vol. 5, no. 10, pp. 3248–3254, Aug. 2008.
- [24] G. Legeay, X. Castel, R. Benzerger, A.-G. Moussavou, R. Sauleau, and M. Guilloux-Viry, "Low-cost photomask fabrication using laser ablation," *J. Mater. Process. Technol.*, vol. 216, pp. 71–78, Feb. 2015.
- [25] E. Carlsson and S. Gevorgian, "Conformal mapping of the field and charge distributions in multilayered substrate CPWs," *IEEE Trans. Microw. Theory Techn.*, vol. 47, pp. 1544–1552, Aug. 1999.
- [26] P. Ren, H. Fan, X. Wang, and X. Tan, "Modified tunable dielectric properties by addition of MgO on $\text{BaZr}_{0.25}\text{Ti}_{0.75}\text{O}_3$ ceramics," *Mater. Res. Bull.*, vol. 46, pp. 2308–2311, Sep. 2011.
- [27] A. Le Febvrier, "Couches minces et multicouches d'oxydes ferroélectrique (KTN) et diélectrique (BZN) pour applications en hyperfréquences," Ph.D. manuscript, University of Rennes 1, Rennes, France, Oct. 2012.
- [28] A.-G. Moussavou, S. Députier, A. Perrin, R. Sauleau, X. Castel, G. Legeay, R. Benzerger, K. Mahdjoubi, and M. Guilloux-Viry, " $\text{KTa}_{0.5}\text{Nb}_{0.5}\text{O}_3$ ferroelectric thin films grown by pulsed laser deposition: Structural characteristics and applications to microwave devices," *Phys. Status Solidi C*, vol. 5, no. 10, pp. 3298–3303, Aug. 2008.
- [29] M. W. Cole, W. D. Nothwang, C. Hubbard, E. Ngo, and M. Ervin, "Low dielectric loss and enhanced tunability of $\text{Ba}_{0.6}\text{Sr}_{0.4}\text{TiO}_3$ based thin films via material compositional design and optimized film processing methods," *J. Appl. Phys.*, vol. 93, p. 9218, Jun. 2003.
- [30] M. W. Cole, E. Ngo, S. Hirsch, M. B. Okatan, and S. P. Alpay, "Dielectric properties of MgO-doped compositionally graded multilayer barium strontium titanate films," *Appl. Phys. Lett.*, vol. 92, p. 072906, Feb. 2008.